

## Supplementary Information

### **Magnetic lanthanide sensor with self-ratiometric time-resolved luminescence for accurate detection of epithelial cancerous exosomes**

Yating Zeng<sup>a,b</sup>, Xuekang Wang<sup>a,b</sup>, Nanhang Zhu<sup>a,b</sup>, Yue Yu<sup>a,b</sup>, Xingyou Wang<sup>a,b</sup>, Ke  
Kang<sup>a,b</sup>, Yao Wu<sup>a,b</sup>, Qiangying Yi<sup>a,b\*</sup>

<sup>a</sup> *National Engineering Research Center for Biomaterials, Sichuan University,  
Chengdu 610064, P. R. China*

<sup>b</sup> *College of Biomedical Engineering, Sichuan University, Chengdu 610064, P. R.  
China*

*Corresponding Author:*

*\*E-mail: qyi@scu.edu.cn (Q.Y.).*

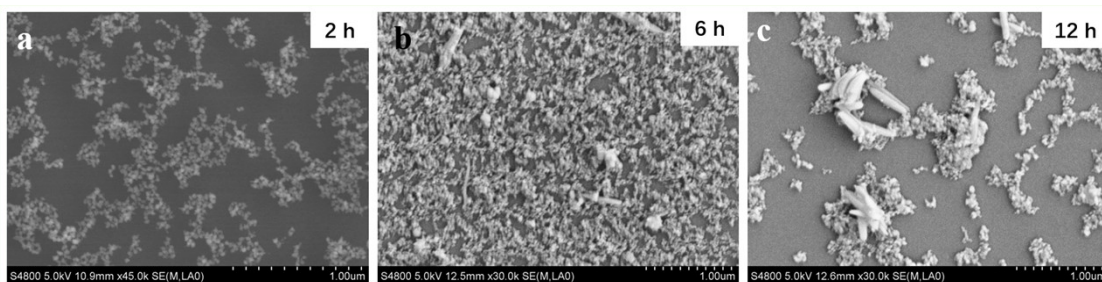


Fig. S1. Different hydrothermal reaction times of  $\text{NaYF}_4:\text{Tb}@PEI$

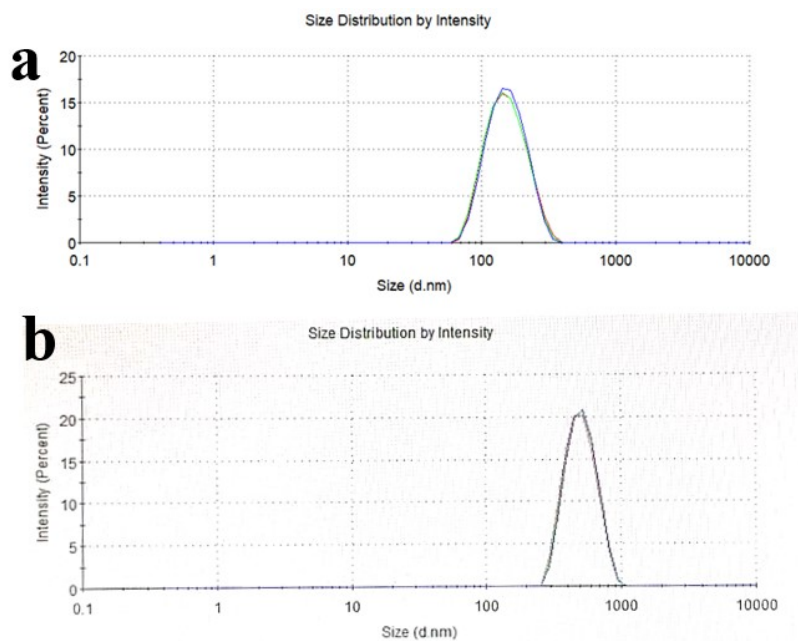


Fig. S2. The hydrodynamic diameter of  $\text{Fe}_3\text{O}_4$  nanoparticles (a) and  $\text{Fe}_3\text{O}_4@\text{NaYF}_4:\text{Tb}$  nanoparticles (b) measured by DLS.

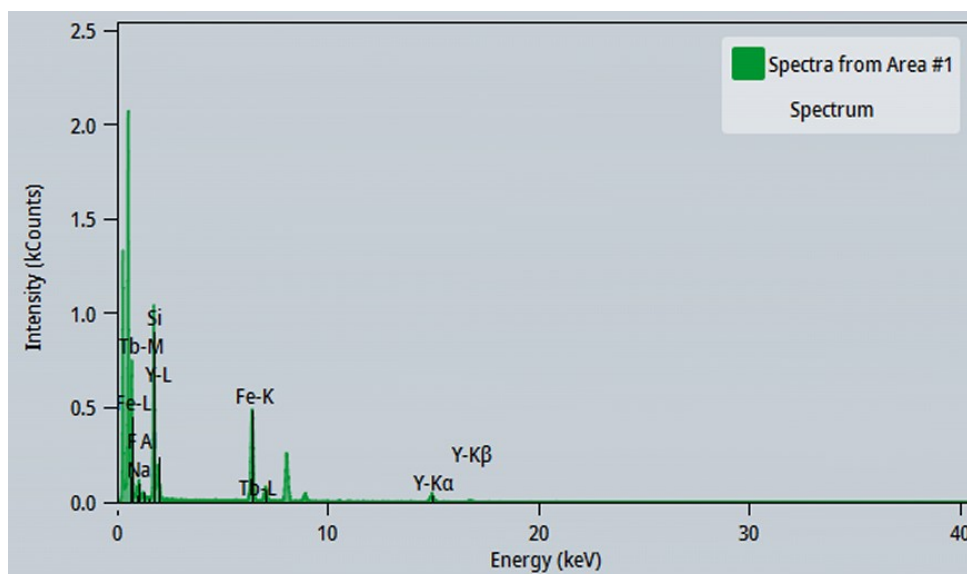


Fig. S3. The EDS analysis for element composition of the  $\text{Fe}_3\text{O}_4@\text{SiO}_2@\text{NaYF}_4:\text{Tb}$ .

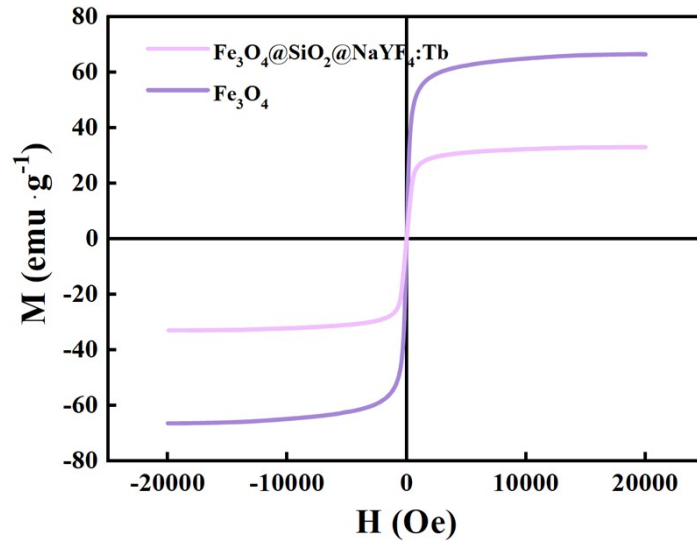


Fig. S4. Magnetic hysteresis loop images of Fe<sub>3</sub>O<sub>4</sub> nanoparticles and Fe<sub>3</sub>O<sub>4</sub>@SiO<sub>2</sub>@NaYF<sub>4</sub>:Tb nanoparticles.

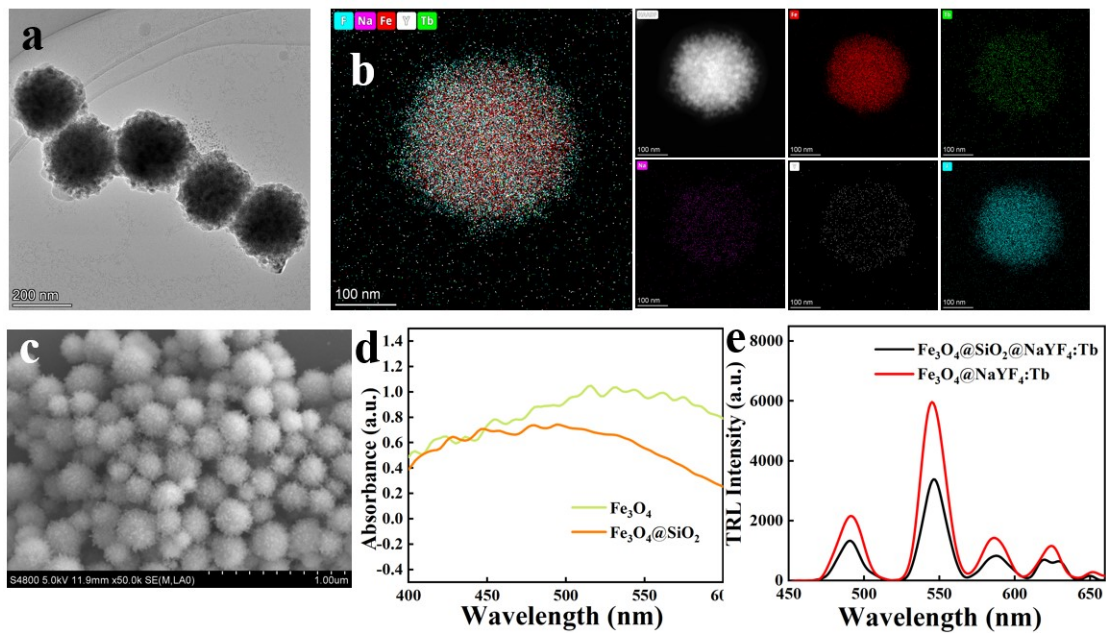


Fig. S5. TEM (a) and SEM (c) images of Fe<sub>3</sub>O<sub>4</sub>@NaYF<sub>4</sub>:Tb nanoparticles. (b) EDS analyses of the Fe<sub>3</sub>O<sub>4</sub>@NaYF<sub>4</sub>:Tb nanoparticles. (d) UV-vis absorbance spectra of Fe<sub>3</sub>O<sub>4</sub> nanoparticles and Fe<sub>3</sub>O<sub>4</sub>@SiO<sub>2</sub> nanoparticles. (e) The time-resolved luminescence spectrum of Fe<sub>3</sub>O<sub>4</sub>@NaYF<sub>4</sub>:Tb nanoparticles and Fe<sub>3</sub>O<sub>4</sub>@SiO<sub>2</sub>@NaYF<sub>4</sub>:Tb nanoparticles.

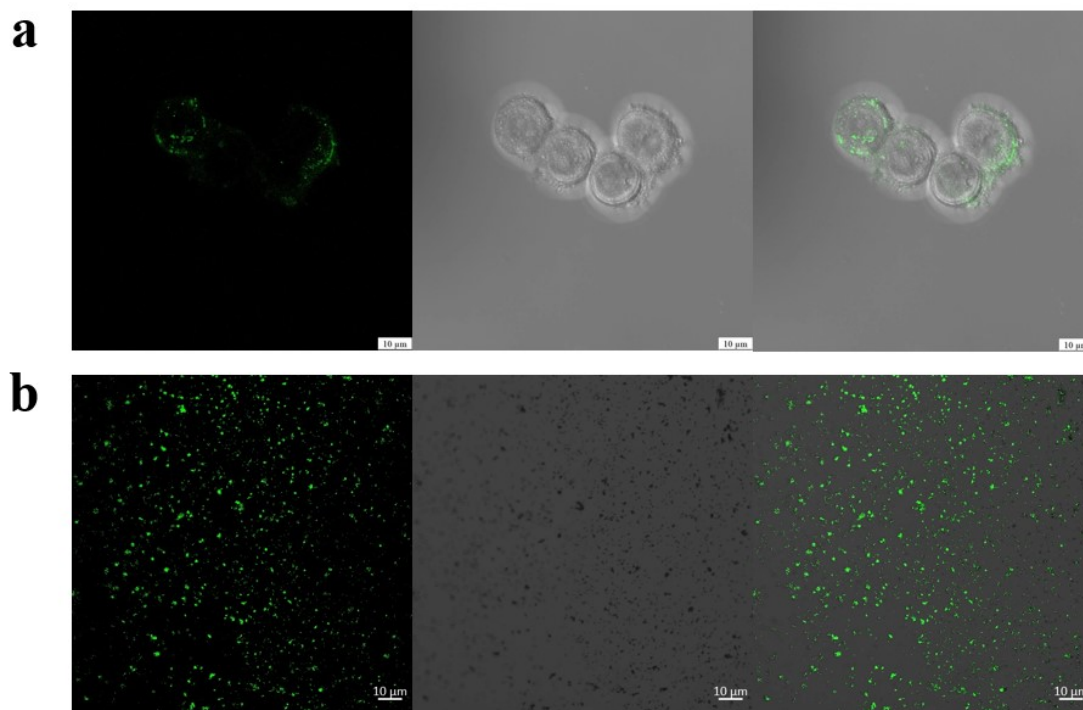


Fig. S6. CLSM images of (a) MCF-7 cells incubated with Apt<sub>EPCAM</sub>-FAM and (b) MLS@Apt<sub>EPCAM</sub>-FAM.

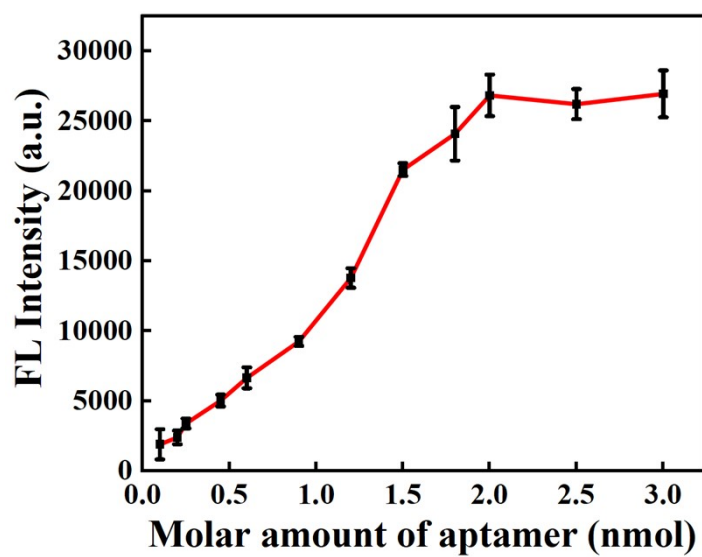


Fig. S7. Optimization of the amount of the Apt<sub>EPCAM</sub> loaded on Fe<sub>3</sub>O<sub>4</sub>@SiO<sub>2</sub>@NaYF<sub>4</sub>:Tb nanoparticles.

### Magnetic recovery efficiency testing of MLS

First, UV-visible absorption spectra (wavelength scan, slit width 5 nm) of MLS at different concentrations were obtained to establish a standard curve. Then, absorbance

values of the supernatant at different magnetic separation times were recorded and the established standard curve was used to calculate the corresponding concentrations and recovery efficiency of MLS:

$$\frac{\text{concentration of MLS before magnetic separation} - \text{initial concentration of MLS}}{\text{concentration of MLS before magnetic separation}} \times 100\%$$

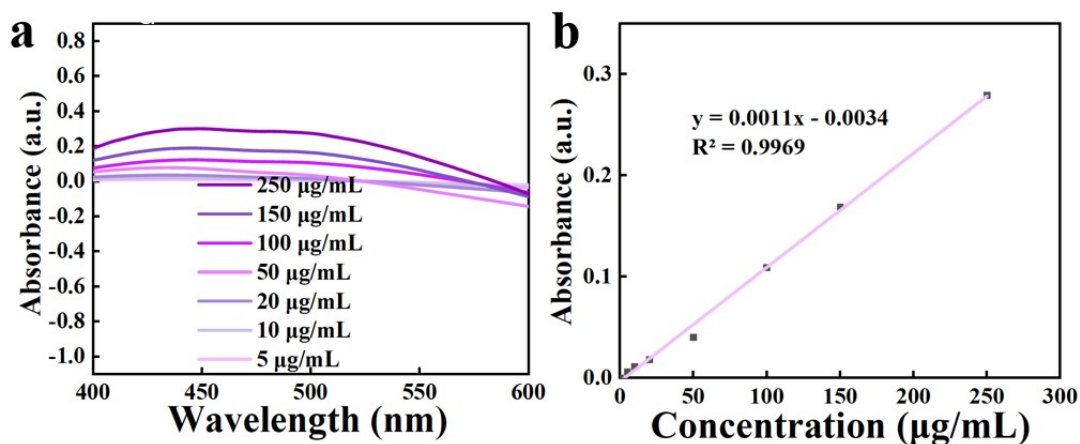


Fig. S8. UV-vis absorbance spectra (a) and (b) corresponding linear relationship of different concentrations of MLS.

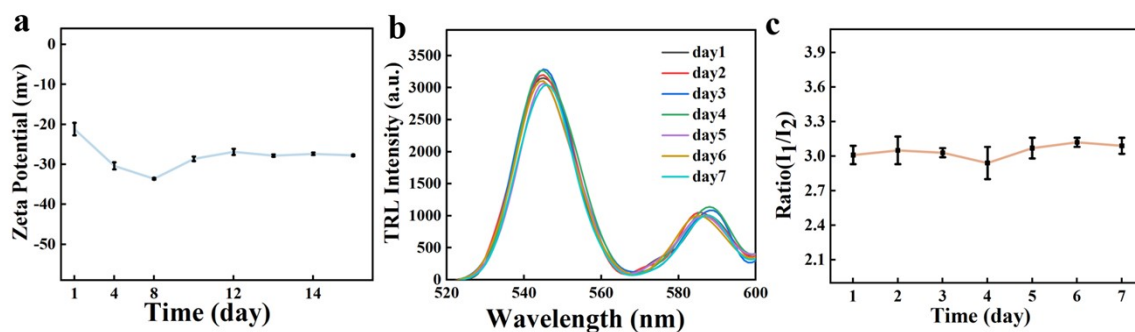


Fig. S9. Storage stability curve of MLS. (a) Zeta potential stability and (b-c) TRL stability.

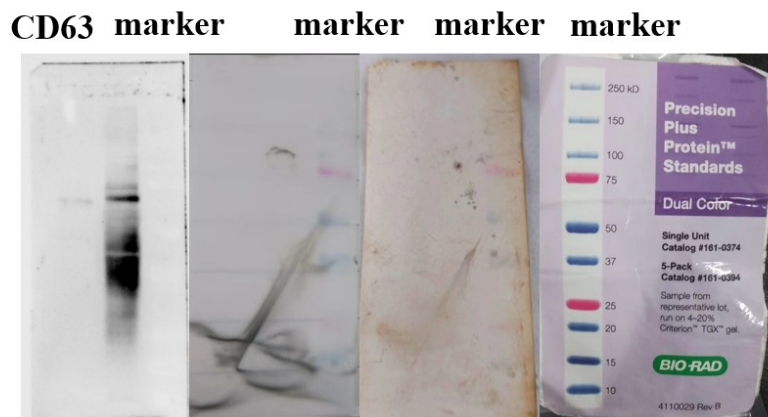
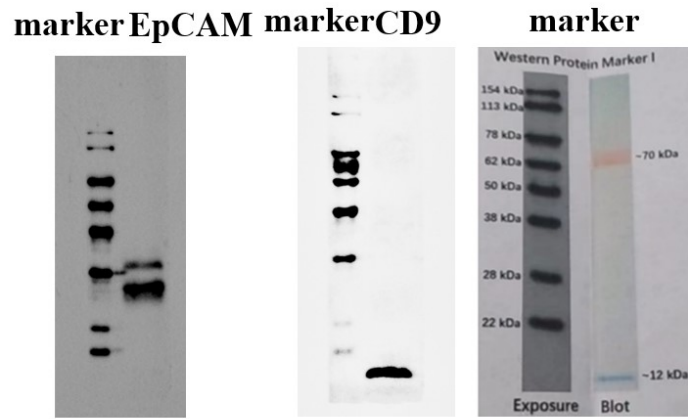


Fig. S10. The raw data of western blotting experiments for demonstrating the two exosomal proteins and one epithelial cancer-associated protein on MCF-7 exosomes.

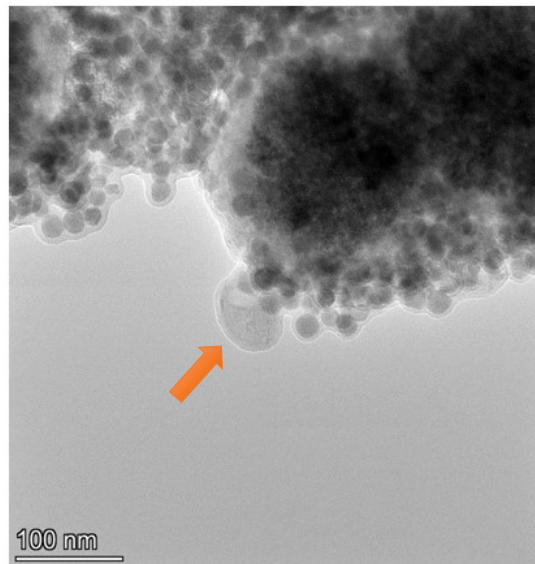


Fig. S11. TEM image of the MLS@exo, and one captured exosome was pointed out by an arrow.

Tab. S1 The TRL intensity experimental results in model samples.

<b>Number of Exosomes</b>	<b>Peak value at 543 nm (I<sub>1</sub>) (repeated 3 times)</b>	<b>Peak value at 583 nm (I<sub>2</sub>) (repeated 3 times)</b>	<b>Ratio (I<sub>1</sub>/I<sub>2</sub>)</b>	<b>Average Ratio</b>	<b>STDEV</b>	<b>RSD (%)</b>
2.3 × 10 <sup>2</sup>	3495	1129	3.096	3.162	0.0605	1.91
	3515	1116	3.150			
	3589	1107	3.242			
2.3 × 10 <sup>3</sup>	3748	1113	3.367	3.369	0.0371	1.10
	3727	1121	3.325			
	3781	1107	3.415			
2.3 × 10 <sup>4</sup>	4040	1132	3.569	3.541	0.0512	1.44
	4038	1164	3.469			
	4047	1129	3.584			
2.3 × 10 <sup>5</sup>	4462	1188	3.756	3.746	0.0325	0.87
	4441	1175	3.779			
	4446	1201	3.702			
2.3 × 10 <sup>6</sup>	4651	1216	3.825	3.822	0.0187	0.49
	4666	1214	3.843			
	4660	1227	3.798			
2.3 × 10 <sup>7</sup>	4941	1252	3.947	3.993	0.0332	0.83
	4993	1241	4.023			
	5002	1248	4.008			
2.3 × 10 <sup>9</sup>	5373	1271	4.227	4.202	0.0178	0.42
	5368	1281	4.190			
	5391	1287	4.189			

\* *STDEV*: Standard Deviation, *RSD*: relative standard deviation.

Tab. S2 Information of clinical samples.

<b>Sample</b>	<b>Type</b>	<b>Gender</b>	<b>Age</b>
<b>H1</b>	Health	Male	31
<b>H2</b>	Health	Male	34
<b>H3</b>	Health	Female	45
<b>H4</b>	Health	Female	28
<b>H5</b>	Health	Female	36
<b>B1</b>	Breast Cancer	Female	48
<b>B2</b>	Breast Cancer	Female	85
<b>B3</b>	Breast Cancer	Female	67
<b>B4</b>	Breast Cancer	Female	50
<b>B5</b>	Breast Cancer	Female	69
<b>L1</b>	Liver Cancer	Female	50
<b>L2</b>	Liver Cancer	Female	58
<b>L3</b>	Liver Cancer	Female	49
<b>L4</b>	Liver Cancer	Male	70
<b>L5</b>	Liver Cancer	Male	50

\



Tab. S3 The TRL experimental results in real samples.

Samples		Peak value at 543 nm (I <sub>1</sub> )	Peak value at 583 nm (I <sub>2</sub> )	Ratio (I <sub>1</sub> /I <sub>2</sub> )	Average Ratio	STDEV	RSD (%)
<b>Health</b>	<b>H1</b>	4480	1320	3.394	3.427	0.155	4.522
	<b>H2</b>	4073	1297	3.140			
	<b>H3</b>	4342	1218	3.565			
	<b>H4</b>	4134	1184	3.491			
	<b>H5</b>	4334	1223	3.544			
<b>Breast cancer</b>	<b>B1</b>	4455	1133	3.932	3.977	0.101	2.554
	<b>B2</b>	4753	1165	4.080			
	<b>B3</b>	4327	1134	3.816			
	<b>B4</b>	4929	1205	4.090			
	<b>B5</b>	5105	1287	3.966			
<b>Liver cancer</b>	<b>L1</b>	4820	1165	4.137	4.253	0.095	2.228
	<b>L2</b>	5196	1235	4.207			
	<b>L3</b>	5272	1205	4.375			
	<b>L4</b>	5334	1273	4.190			
	<b>L5</b>	5031	1155	4.356			
<b>RSD between the health and breast cancer (%)</b>							7.429
<b>RSD between the health and liver cancer (%)</b>							10.758
<b>RSD between breast cancer and liver cancer (%)</b>							4.120

\* *STDEV*: Standard Deviation, *RSD*: relative standard deviation.